Direct CO_2 conversion to syngas in a $BaCe_{0.2}Zr_{0.7}Y_{0.1}O_{3-\delta}$ - based proton-conducting electrolysis cell

*Nuria Bausá, Sonia Escolástico and José M. Serra**

Instituto de Tecnología Química (Universitat Politècnica de València – Consejo Superior de Investigaciones Científicas), Av. Naranjos s/n, E-46022 Valencia (SPAIN)
* to whom correspondence should be addressed, Fax 0034.963.877.809
e-mail: jmserra@itq.upv.es

ABSTRACT

Electrolysis of steam and CO_2 is considered to be a promising instrument for energy storage via sustainable H_2 and hydrocarbon production. A model electrolysis cell was assembled using a thick $BaCe_{0.2}Zr_{0.7}Y_{0.1}O_{3-\delta}$ (BCZY27) electrolyte and two distinct electrodes, i.e., a (H_2-cathode) porous Pt layer; and (steam-anode) a composite made of 60 vol. % $La_{0.8}Sr_{0.2}MnO_{3-\delta}$ (LSM) and 40 vol. % BCZY27. The as-sintered steam electrode was catalytically-activated with Pr_2O_7-CeO_2 nanoparticles. The cell was characterized by means of voltamperometry and impedance spectroscopy. Different operation parameters were analysed: temperature; water concentration in the anode chamber; and H_2 and CO_2 concentration in the cathode chamber. Increasing H_2O concentration (in the anode) and presence of CO_2 (in cathode) positively affected the electrode performance giving rise to lower cell overpotential and, consequently, substantial improvement in Faradaic efficiency. The high electrolyte thickness and the non-optimized Pt cathode limited the range of current density and the achieved peak power densities. The Faradaic efficiency for water electrolysis reached a value of 39% at 10.4 mA/cm^2, as determined by the analysis of the H_2 production. During co-electrolysis, the CO_2 reaction was fostered by co-feeding a minimum H_2 amount. CO formation took place through the reverse water gas shift (RWGS) reaction. When the current density was applied, CO_2 conversion increased due mainly to the non-Faradaic electrochemical modification of catalytic activity (NEMCA effect) that allowed for the improvement of CO_2 hydrogenation kinetics.

KEYWORDS

Proton ceramic electrolyzer cell (PCEC), electrolysis, co-electrolysis, BCZY, catalytic nanoparticles; CO_2

1. Introduction

High temperature electrolysis (HTE) makes possible the efficient and environmentally-friendly production of H_2 and hydrocarbons by the combined use of renewable electricity and available sources of heat and steam from non-fossil energy sources such as solar and geothermal energy. Most research to date is based on Solid Oxide Electrolyzer Cells (SOECs) that use oxide-ion conducting electrolytes operated at ~800 °C. SOECs are a mature technology that produces H_2 on the steam feed side, and thus requires separation and drying of the H_2, increasing energy costs and plant complexity[1-3].

During the last decade, Proton Ceramic Electrolyzer Cells (PCECs) have been widely studied and received significant attention [4-8]. In comparison with SOECs, high temperature Proton Conducting Electrolyzer Cells (PCEC) transport protons from the steam side to the cathode, releasing O_2 on the steam side and producing dry H_2 at the cathode. Subsequently, PCECs require less separation process stages than SOECs. In addition, protons exhibit lower activation energies than oxide ions, and ceramic proton conductors are able to operate at lower temperatures (500 – 700 ºC).

PCECs, like SOECs, may also be useful for the electrochemical reduction of CO_2 to CO giving rise to a syngas stream by partial reduction and hydrogenation of the CO_2 stream. In contrast to SOECs, pressurised steam and CO_2 are fed on separate sides of the cell in the PCEC, which may be advantageous[9-12]. A strong benefit of PCEC operation is that dry H_2 is produced in the anode while it is not necessary to pressurize the steam. The mechanical/thermal steam compression utilized in SOEC could be replaced by the electrochemical compression of protons/hydrogen pumped into the anode. However, most of the previous work is focused on the co-electrolysis of steam and CO_2 using SOECs.

Among proton conducting ceramics, doped $BaCeO_3$ and $BaZrO_3$ based oxides are the most widely studied electrolyte materials due to their high proton conductivity. Barium cerates ($BaCeO_3$) exhibit higher proton conductivity than barium zirconates ($BaZrO_3$), nevertheless, $BaCeO_3$-based materials are reported to suffer chemical instability under CO_2-containing atmospheres due to the formation of barium carbonate ($BaCO_3$) and

cerium oxide (CeO_2). $BaZrO_3$-based materials are the most suitable to work in these conditions because of their stability in CO_2 atmospheres despite having lower proton conductivity[13, 14] due to their significant grain boundary resistance. However, high sintering temperature is needed to achieve dense samples, which causes Ba evaporation and the subsequent loss of transport properties. To overcome the disadvantages of both materials, solid solutions of doped $BaCeO_3$ and $BaZrO_3$ have been widely investigated[15-17].

Most of the reported PCEC studies employ an electrolyte material based on these solid solutions. Recently, J. Dailly *et al*. validated electrical performance beyond 400 mW/cm^2 at 600–700 ºC for a few hundred hours of stable operation under a dynamic fuel cell power demand profile using $BaCe_{0.9}Y_{0.1}O_{3-\delta}$ (BCY)-based proton conducting ceramic cells [18-21]. Ruiz-Trejo and Irvine successfully carried out steam and CO_2 co-electrolysis with a button PCEC cell around 500 ºC, with Pt as both the cathode and the anode for a few hours[9, 10]. Xie et al. obtained promising results by using $BaCe_{0.5}Zr_{0.3}Y_{0.16}Zn_{0.04}O_{3-\delta}$ as an electrolyte[22].

In this work, the selected electrolyte material is based on $BaZrO_3$ where Y and Ce are incorporated to produce $BaCe_{0.2}Zr_{0.7}Y_{0.1}O_{3-\delta}$ (BCZY27). Y is added to promote oxygen vacancies/proton incorporation while Ce is added to improve the proton conductivity and sintering [23-26]. This material, BCZY27, is a promising material to be implemented in electrochemically-driven catalytic membrane reactors as has been demonstrated in previous studies on methane dehydro-aromatization and steam methane reforming [27, 28].

This work presents the study of a proton ceramic electrolyzer cell by using a BCZY27 electrolyte and a composite formed by LSM/BCZY27 60/40 vol. % infiltrated with Pr_2O_7-CeO_2 as an anode while a porous Pt layer is used as the cathode. The cell was characterized by means of voltamperometry (i-V curves) and Electrochemical Impedance Spectroscopy measurements (EIS) in both fuel cell and electrolysis modes. Furthermore, different operation parameters were analyzed: temperature, H_2O concentration in the anode chamber, H_2 and CO_2 concentration in the cathode chamber. Electrolysis and co-electrolysis experiments were performed at 700 ºC and the Faradaic efficiency was

determined. Moreover, this study aims to provide further understanding about the co-electrolysis principles for further operation in larger PCECs setups.

2. Experimental

Electrolysis measurements were performed using a dense $BaCe_{0.2}Zr_{0.7}Y_{0.1}O_{3-\delta}$ (BCZY27) electrolyte with a thickness of 500 μm. The electrolyte was obtained by mixing the BCZY27 powder (provided by CerPoTech) with 1 wt. % ZnO (Sigma Aldrich) that acts as sintering aid [29, 30] and ball-milled for 16 h in acetone. Subsequently, the electrolyte was uniaxially pressed at ~120 MPa and calcined in air at 1550 °C for 12 h with a constant heating rate of 2 $^{o}C \cdot min^{-1}$. The electrolyte was sintered using a BCZY27 powder bed previously sintered at 1550 °C and polished before applying the electrodes. The diameter of the electrolyte after sintering was 15 mm.

A Pt porous layer with a thickness of 10 μm and a particle size of ~ 1 μm (see Supporting Figure S1) was used as the cathode and was deposited by screen-printing an ink (MaTecK) with a Pt particle size range of 0.2 – 1.8 μm. A composite formed by 60 vol. % $La_{0.8}Sr_{0.2}MnO_{3-\delta}$ (LSM, Marion Technologies) and 40 vol. % BCZY27 was used as the anode, both the Pt and the composite were sintered at 1100 ^{o}C for 2 h. An LSM/BCZY backbone composite was selected due to its good adherence onto the electrolyte and its stability under oxidizing conditions[6]. Powders were ball-milled for 16 h in acetone to homogenize the grain size. Then, inks were prepared by using terpineol and ethylcellulose in a three-roll mill. Porous electrodes were obtained by screen-printing the inks over the surfaces of the BCZY electrolyte. The diameter of the round electrodes was 7 mm.

LSM/BCZY27 60/40 vol. % backbone electrode was infiltrated with a 2 M solution (ethanol-water) prepared with Pr and Ce precursors to improve the catalytic activity of the anode. The solution was dropped onto the whole electrode surface and was covered with a Pr_2O_7-CeO_2 infiltrated oxide catalyst after being calcined at 850 ^{o}C for 2 hours. Previous works reported an electrode kinetics enhancement of more than one order of magnitude after being infiltrated [31].

Electrochemical measurements, electrolysis and co-electrolysis experiments were performed in a double-chamber quartz reactor. The cell was sealed to the reactor by using an Ag-based gasket that allowed the sealing to be done at a moderate temperature. The

set-up allows for working with different gases in dual atmosphere and in a broad range of temperatures.

The cell was electrochemically characterized by means of i-V curves, Open Circuit Voltage (OCV) and electrochemical impedance measurements (EIS). The electrochemical measurements were carried out using a Solartron Analytical 1470E CellTest System and ZView software was used for EIS fitting. Cell performance was evaluated in fuel cell and electrolysis mode, studying different parameters: (1) temperature, (2) H_2O concentration in the anode chamber, (3) H_2 concentration and (4) CO_2 concentration on the cathode side.

In the electrolysis experiments, Ar (100 mL/min) was fed on the cathode chamber whereas the anode side was exposed to 100 mL/min of synthetic air. Synthetic air was saturated in water at different temperatures, obtaining steam concentrations of 3% (25 °C) and 7.5% (50 °C). A constant current was passed through the cell for 40 minutes, ranging from 1 to 5 mA (2.60 to 13 mA/cm^2). For co-electrolysis experiments, the cathode chamber was fed with 9 % CO_2 in Ar whereas in the anode chamber humidified air was fed (7.5% H_2O).

The H_2 production and concentration of the formed products in the cathode were analyzed by using a Micro-GC CP-4900 gas chromatograph equipped with Molsieve5A and PoraPlot-Q glass capillary modules to determine the Faradaic efficiency of the reactions. Flow rates expressed as mL·min^{-1} were calculated at standard conditions.

The Faradaic efficiency (η_F, eq. 1) was calculated from the theoretical H_2 production ($F(H_2)_{th}$, eq. 2) determined by the Faraday's equation and the obtained H_2 flow quantified by gas chromatography $F(H_2)_{exp}$.

$$\eta_F = \frac{F(H_2)_{exp}}{F(H_2)_{th}} \qquad (1)$$

$$\text{where } F(H_2)_{th} = \frac{I}{nF} \qquad (2)$$

n is the number of the transferred electrons and *F* the Faraday constant.

3. Results and discussion

3.1. Electrochemical performance

The electrochemical performance of the cell was evaluated under different conditions: (1) temperature: 700, 650 and 600 ºC, from the highest to the lowest temperature; (2) steam concentration in the anode chamber: 3 and 7.5% H_2O; (3) CO_2 presence in the cathode chamber; and (4) H_2 concentration in the cathode chamber: 10, 20 and 30%. In all measurements, a gas flow rate of 100 mL/min (pure Ar or a mixture of H_2, CO_2 and Ar) was fed to the cathode side and 100 mL/min of synthetic air saturated in H_2O (3 or 7.5%) was delivered to the anode side.

i-V curves and the corresponding power densities in fuel cell mode at 700 ºC using 10% H_2 in the cathode and synthetic air with two different H_2O concentrations in the anode are shown in Figure 1a. The OCV is relatively low when 3% H_2O is fed to the anode. The low OCV values could be ascribed to (i) gas leakage between both sides of the cell due to sealing issues or (ii) electronic leakage due to significant electronic conductivity in BCZY27 under these conditions as was previously observed for $BaCe_{0.5}Zr_{0.3}Y_{0.16}Zn_{0.04}O_{3-\delta}$[10]. Gas leaks were checked by feeding He as a gas tracer in the anode chamber and analyzing the He in the cathode chamber. The gas leakage was found to be very small as Helium was not detected in the cathode chamber. Therefore, gas leakage was not responsible for the low OCV value. On the other hand, OCV increased up to 0.9 V when H_2O concentration was increased to 7.5%. This effect is ascribed to the drop in the electronic conductivity at higher steam concentrations mediated by the higher hydration degree of the electrolyte. BCZY27 at 700 ºC behaves as a pure ionic conductor under reducing conditions whereas under oxidizing atmospheres *p*-type electronic conduction becomes very significant [8, 23, 32].

i-V curves are almost linear suggesting that the ohmic regime is dominant under these conditions. No charge transfer activation or gas concentration polarization effects are visible. The peak power densities are about 1.2 and 4.3 $mW \cdot cm^{-2}$ with 3% and 7.5 % H_2O, respectively. These low values may be related to the high thickness (500 μm) of the electrolyte and the non-optimized Pt cathode, with limited triple-phase boundary points for H_2 evolution reaction.

The performance of the fuel cell was further evaluated by feeding CO_2 to the cathode. Figure 1b shows the effect produced by the CO_2 addition on the i-V curves and the power densities at 700 ºC. The addition of CO_2 to the cathode has no effect on the OCV but it enables the improvement of the peak power density, reaching values up to 5.9 $mW \cdot cm^{-2}$. This positive effect could be ascribed to (1) higher water concentration in the cathode –

formed via RWGS[1]-, which may positively affect the electrolyte conduction and electrode kinetics; and (2) direct CO_2 effect in the kinetics of H_2 evolution mechanism. The expected OCV values in electrolysis and co-electrolysis mode at different steam concentrations are given in Supporting Figure S3.

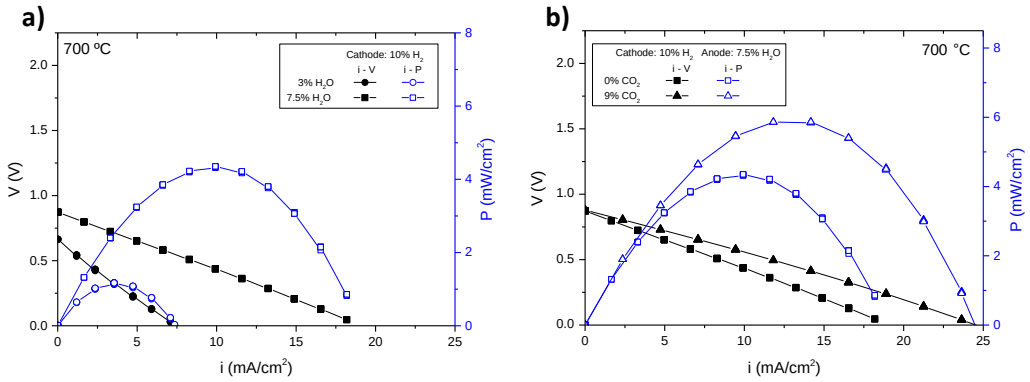

Figure 1. (a) Fuel cell polarization curves at 700 °C by feeding: (a) 10% H_2 in Ar in the cathode side and synthetic air with 3% and 7.5 % steam in the anode. (b) 10% H_2 in Ar with (9%) and without CO_2 in the cathode side and wet synthetic air (7.5 % H_2O) in the anode.

Impedance spectra under fuel cell mode near the OCV were recorded under different conditions to study the nature of the electrochemical steps contributing to cell resistance. Figure 2 shows the EIS spectra, the polarization resistance (Rp) and the electrolyte conductivity extracted from the corresponding impedance spectra under different atmospheres and temperatures. EIS measurements were fitted by using the equivalent circuit $LR_1(R_2Q_2)(R_3Q_3)$ where R_1 (real resistance) corresponds to the bulk transport whereas R_2Q_2 and R_3Q_3 are assigned to the electrode processes due to their associated capacitance and frequency range. The EIS spectra not only highlights the strong influence of the electrodes on the cell performance, but also the important resistance of the electrolyte. In fact, the electrode resistance is almost the same as the electrolyte resistance. It should be pointed out that the steam/air electrode was previously optimized and the corresponding polarization resistance at 700 ºC under 2.25 bar H_2O and 0.75 bar air (75%-H_2O/air, LSM/BCZY27 | BCZY27 | LSM/BCZY27, 75%-H_2O/air) was lower than 1 $\Omega \cdot cm^2$ at OCV. Consequently, the high polarization resistance obtained in the cell is mainly ascribed to the Pt H_2 electrode (electrolysis cathode) that provides a high electrode resistance[33].

[1] RWGS states for Reverse Water-Gas Shift reaction: $CO_2 + H_2 \leftrightarrow CO + H_2O$

The polarization resistance slightly decreases with both, H_2 and CO_2 concentration. The drop of the Rp with H_2 concentration is attributed to the enhancement of the Pt electrode kinetics as has been previously reported[34]. On the other hand, the decrease of the Rp with the addition of CO_2 to the cathode can be ascribed to the improvement of the Pt electro-catalytic activity which is analogous to what was observed for Fe based electrodes[10]. BCZY27 conductivity remains almost constant with the variation of H_2 concentration due to the prevailing protonic conductivity under the studied conditions whereas it improves with the presence of CO_2. This increase can be associated with the concomitant transport of oxide ions under reducing atmospheres and the higher hydration degree due to the water formation via RWGS. Thus, the improvement of the cell performance by feeding CO_2 (Figure 1b) is attributed to both the decrease of the ohmic resistance of the electrolyte and the decrease of the polarization resistance of the cathode.

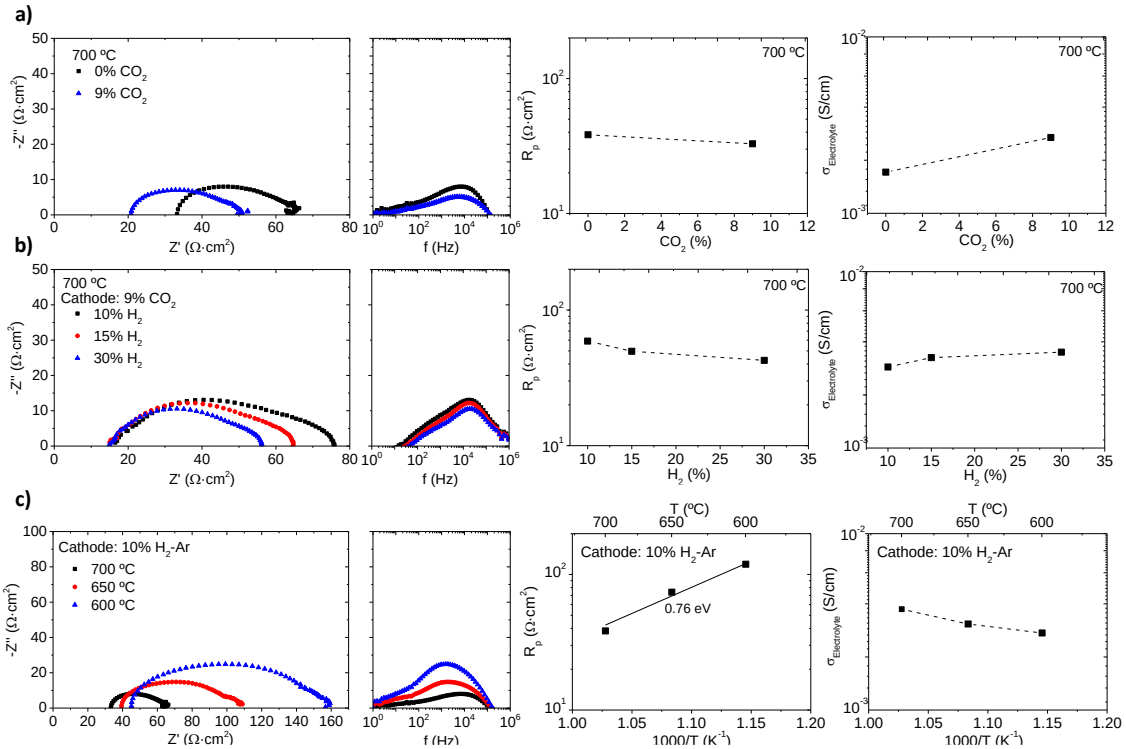

Figure 2. EIS measurements including Nyquist and Bode plots, electrodes polarization resistance (R_p) and total conductivity of the electrolyte at 700 ºC: (a) feeding 10% H_2 in Ar with or without CO_2; (b) feeding 9% CO_2 and different concentrations of H_2 in the cathode; and (c) as a function of the temperature by feeding 10% H_2 in Ar in the cathode. Anode was fed with wet synthetic air (7.5 % H_2O) in all the studied conditions.

The i-V and i-P curves (Figure 3a-b) plotted as a function of the temperature revealed the expected thermal-activation behavior with and without CO_2. In particular, R_p is mainly responsible for the worsening cell performance due to the increase in resistance when

temperature decreases. This fact is also visible in Figure 2c where the impedance spectra and the corresponding R_p as a function of the temperature measured in the LSM/BCZY27 | BCZY27 | Pt cell fed with 10% H_2 in Ar and air with 7.5% H_2O are shown. The activation energy (E_a) for the cell corresponds to 0.76 eV indicating that proton conduction across the BCZY27 phase in the composite anode is not the rate-limiting step since the expected activation energy for proton migration ranges between 0.4 and 0.6 eV.

When CO_2 is added to the cathode stream (Figure 3b), the performance of the cell improves at all tested temperatures, i.e. the peak power density increases around 34%, 24% and 6% at 700 ºC, 650 ºC and 600 ºC, respectively, as compared with the CO_2-free results. The positive effect of the CO_2 on the cathode side is attributed to both, the higher hydration degree of BCZY27 and the transport of oxide ions –in addition to protons– in the electrolyte as was previously explained which could enable the adjustment of the CO/H_2 ratio in the produced dry syngas.

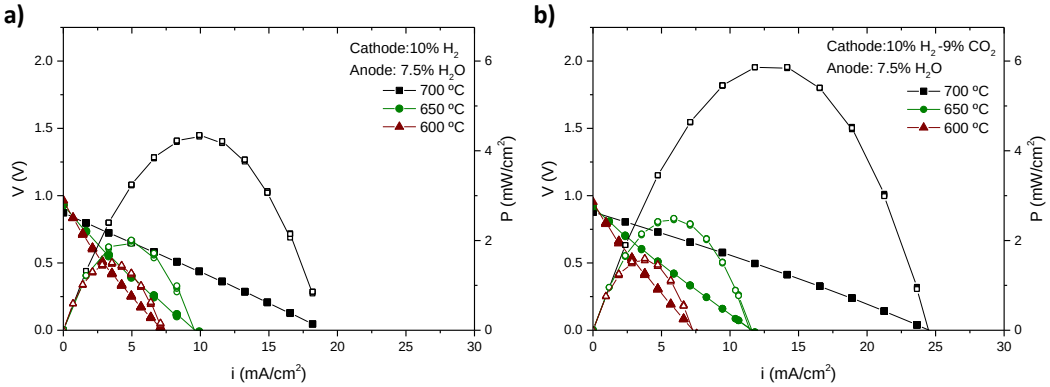

Figure 3. Fuel cell polarization curves at different temperatures feeding wet synthetic air (7.5 % H2O) in the anode and (a) 10% H_2 in Ar and (b) 9% CO_2-10% H_2 in Ar in the cathode.

i-V curves in electrolysis mode are shown in Figure 4. The current density possesses a negative sign indicating that the current is applied to the electrolyzer. Similar to the fuel cell mode, the rise in water concentration (from 3% to 7.5% H_2O) improves the cell performance as can be observed in Figure 4a (10% H_2 in the cathode). As previously discussed, this improvement is related to two effects, the increase of the protonic conductivity related to the higher oxide hydration, and to a lesser extent, the associated decrease of the electronic conductivity of the BCZY27 electrolyte [23]. Two regions can be observed when 3% H_2O is fed: low and medium current (up to -8.25 mA/cm^2) and high current, with a slope of 64.78 and 56.11 Ω·cm^2, respectively. On the contrary, a

linear behavior is observed at higher H_2O concentration with a slope of 50.29 $\Omega \cdot cm^2$. These results highlight the importance of the H_2O concentration in the cell performance.

The cell performance was also evaluated by feeding CO_2 to the anode (co-electrolysis mode). For this purpose, a flow rate of 9 mL/min of CO_2 and 10 mL/min of H_2 (balanced with 81 mL/min of Ar) were added to the cathode side whereas a flow rate of 100 mL/min of synthetic air saturated in water (7.5% H_2O) was used in the anode. Figure 4b displays a comparative of the i-V curves obtained with and without the addition of CO_2 to gas in the Pt cathode. CO_2 causes an improvement in electrolysis mode and for fuel cell mode as well. Only one regime can be distinguished for both measurements. The slope of the co-electrolysis is 27.7 $\Omega \cdot cm^2$, significantly lower than that which corresponds to the electrolysis process. Thus, the co-electrolysis process gives rise to lower overpotentials, which allows for operation at higher current densities and subsequently, an improvement of the Faradaic efficiency is expected. In fact, a difference of 0.57 V exists when a current density of 25.8 mA/cm^2 is used. From these results, it can be deduced that co-electrolysis is more kinetically favorable than electrolysis which has been reported previously for conventional SOECs[35] while the additional hydration effect is observed in PCECs.

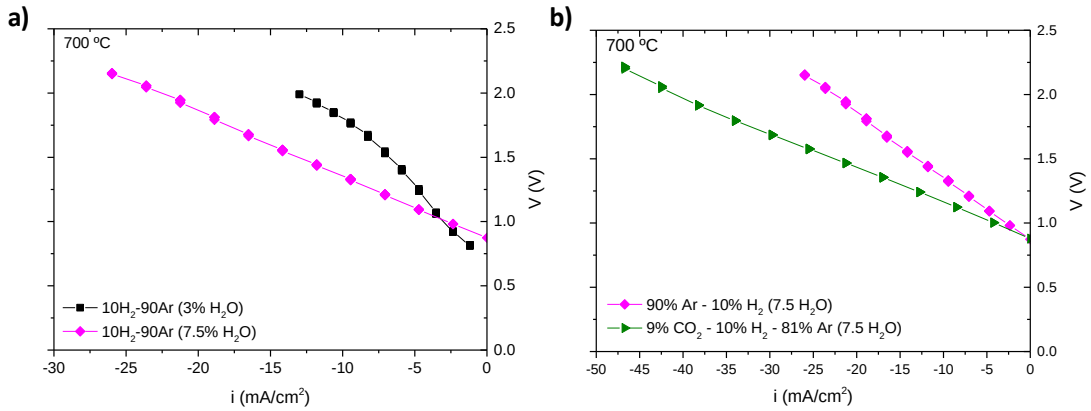

Figure 4. i-V curves in electrolysis mode by feeding (a) different concentrations of water in the anode and (b) different concentrations of CO_2 in the cathode.

In summary, Figure 5 shows the i-V curves in both, fuel cell mode and electrolysis mode, where the improvement of the performance by increasing the water concentration (Figure 5a) and adding CO_2 (Figure 5b) is clearly observed in both modes.

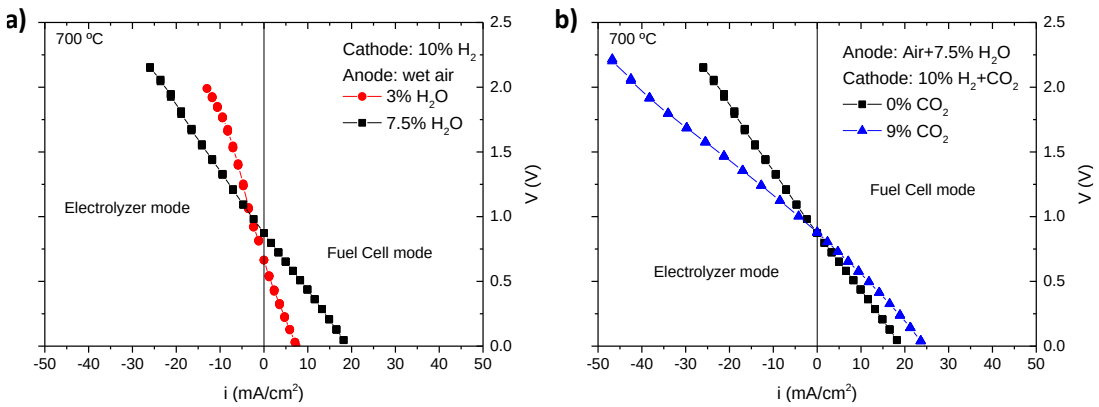

Figure 5. i-V curves in electrolyzer and fuel cell mode under different water concentration (a) and different CO_2 concentration (b).

3.2. Electrolysis and co-electrolysis product analysis

After the electrochemical characterization of the cell, water electrolysis was performed at 700 ºC. The cathode was fed with 100 mL/min of Ar and a flow of 100 mL/min of synthetic air saturated in H_2O (with a concentration of steam of 3 and 7.5%) was introduced in the anode. Different current densities were applied for intervals of 40 minutes. Between each step, no current density was applied. The produced H_2 in the cathode was monitored and quantified continuously by using a gas spectrometer.

Figure 6 plots the H_2 flux produced by water electrolysis at 700 ºC feeding 3% (a) and 7.5% (b) H_2O in the anode. The current densities (mA/cm^2) imposed in each step are shown in the graph. H_2 is detected even at low current densities (5.2 mA/cm^2) and the produced flow increases with the imposed current density. The H_2 production has a very quick response when the current is applied as can be observed in Figure 6b which plots the H_2 flux and the overpotential produced at different current densities (7.5% H_2O in the anode). The stability of the H_2 production and the fast response when the current density is applied are both noteworthy.

The obtained H_2 fluxes are lower than the values reported by Kobayashi et al.[33] in which the cell was fed with humidified air (20% H_2O) to the anode and humidified 1%-H_2/Ar gas (3% H_2O) to the cathode. One of the main reasons for this high performance is the higher conductivity of the electrolyte used by Kobayashi, BZCY442, approximately 0.021 S/cm at 700ºC whereas the BCZY27 used in this study is less acceptor-doped and has a conductivity of around 0.0025 S/cm (as it is observed in Figure 2), practically one order of magnitude lower. Furthermore, the polarization resistance of the electrodes is

lower. In addition to the transport properties of the cell, the water flow rate and concentration is higher in the work of Kobayashi et al. and the concentration of H_2O has a strong influence in the cell performance of the cell.

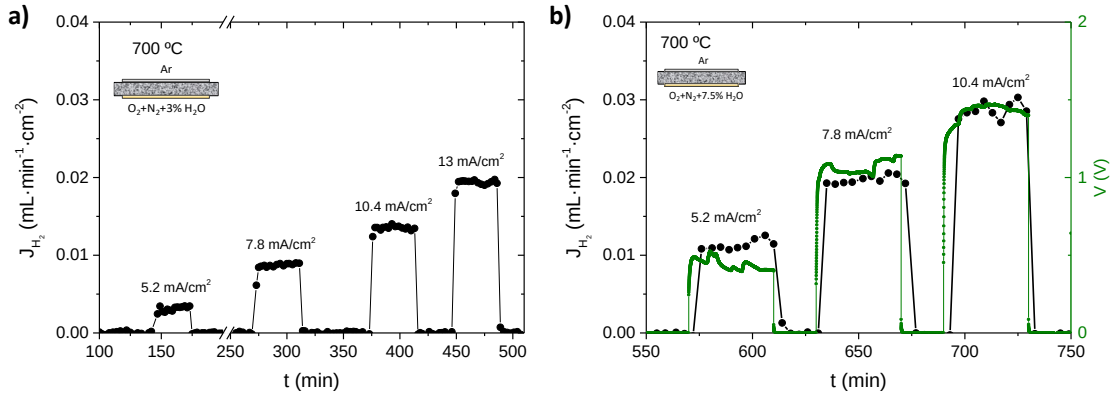

Figure 6. H_2 flux produced by water electrolysis at 700 °C by feeding: (a) 3% water and (b) 7.5% water and the overpotential. Current densities applied are indicated in the graph.

H_2 flow and Faradaic efficiency as a function of the imposed current density and water concentration in the anode are plotted in Figure 7. Both the produced H_2 flow and the Faradaic efficiency increase with the applied current density. Faradaic efficiency ranges between 7 and 21% when 3% H_2O is fed to the anode whereas it improves significantly at higher H_2O concentrations, up to 39% at 10.4 mA/cm^2.

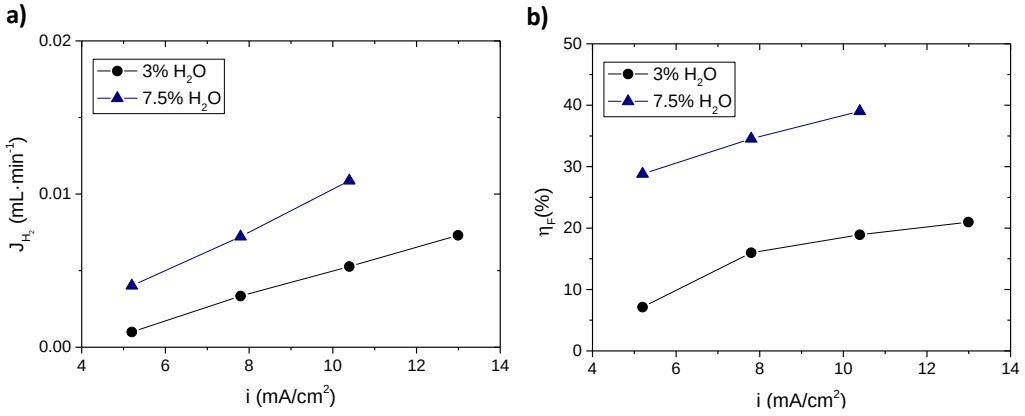

Figure 7. H_2 flow production (a) and Faradaic efficiency (b) as a function of the applied current density and water concentration.

A procedure similar to what was the used for electrolysis was performed for the co-electrolysis test. In this case, a flow of 9 mL/min CO_2 in Ar (total flow=100mL/min) was fed to the cathode side whereas 100 mL/min of humidified synthetic air (7.5% H_2O) were

introduced in the anode. The products obtained in the co-electrolysis were quantitatively analysed by gas chromatography.

Under the abovementioned conditions, no formation of CO or H_2O was detected by the GC analysis, which is attributed to CO and H_2O concentrations below the detection limit of the GC. Subsequently, 5 mL/min of H_2 were added to the cathode stream in order to promote the CO_2 reaction and obtain higher conversions which allows for the quantification of the products concentration.

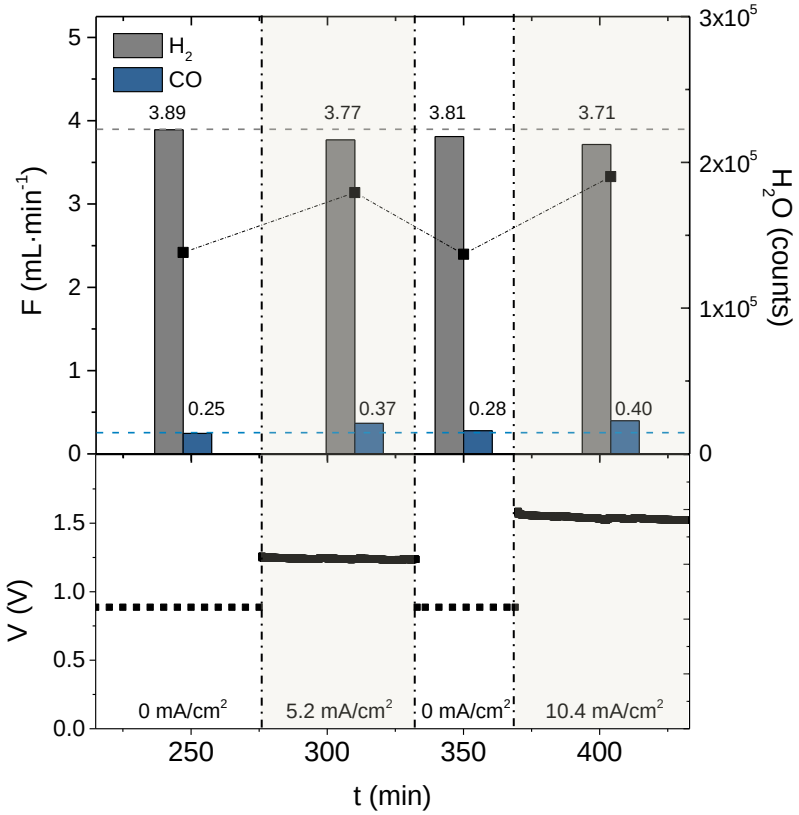

Figure 8. Co-electrolysis results: CO and H_2 flows (bars) and counts of the H_2O detected in the cathode side; voltage of the cell during the co-electrolysis experiment.

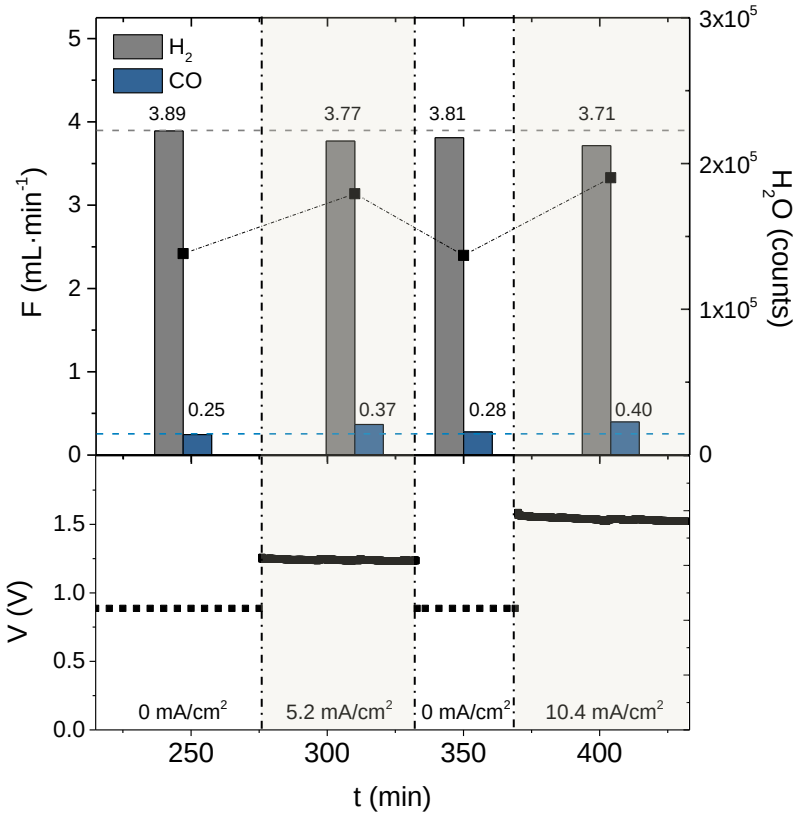

Figure 8 plots the H_2 and CO flows and the H_2O counts after 30 minutes under stream as well as the cell voltage as a function of time and the current density. CO and H_2O are detected as products when no density current is applied due to the RWGS reaction. When current density is applied, H_2 and CO_2 (not shown) concentrations drop, giving rise to higher concentrations of CO and H_2O. When 5.2 mA/cm^2 are applied, the CO_2 conversion increases from 15.0 to 17.8 % and the CO rate enhancement ratio is 1.53 and 1.75 at 5.2 and 10.4 mA/cm^2, respectively. This improvement is higher than the expected due to the H_2 flux electrochemically-pumped through the electrolyte, with a maximum of 0.011 mL·min^{-1} at 10.4 mA·cm^{-2} in electrolysis conditions (see Figure 7, electrolysis conditions). This electrochemical promotion of catalysis is known as non-Faradaic electrochemical modification of catalytic activity (NEMCA effect [36]). Without current, the CO is formed on the Pt electrode. When the current is imposed, the catalytic activity of the Pt surface chemistry is changed and the reaction is further facilitated by the electrochemical spillover of ions from the electrolyte to the electrocatalyst surface (Pt).

Hence, the formation rate increases due to boosted catalytic and electrocatalytic reactions [37, 38].

These results confirm that co-electrolysis of CO_2 and H_2O using a BCZY based electrolyzer cell is a promising technique for syngas production. However, thinner electrolytes and anodes with higher electro-catalytic properties should be developed in order to achieve higher efficiencies and yields.

3.3.Microstructural study of the tested electrolysis cell

The porous cathode (Pt layer) shows a good attachment to the electrolyte surface after the measurements as is observed in Figure 9a. Figure 9b shows a cross-sectional SEM image of the interface between the dense electrolyte (BCZY27) and the anode (LSM/BCZY27). Figure 9c illustrates the backbone electrode filled by needle-like crystals about 200 nm in length of the Pr_2O_7 and round nanoparticles corresponding to the CeO_2 showing good dispersion of the catalyst in the anode (see Supporting Figure S2) [31, 39, 40].

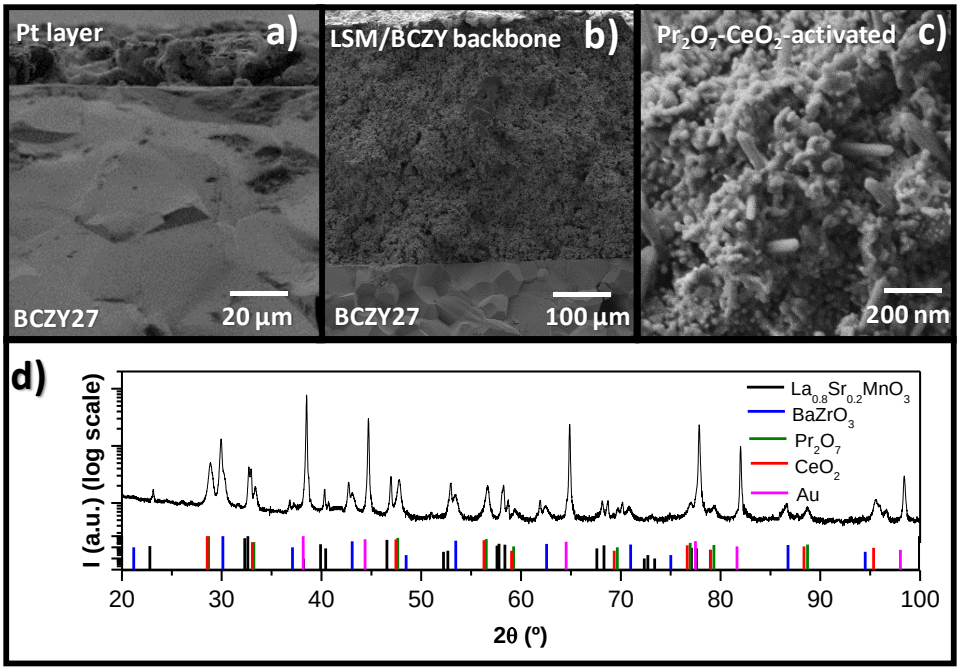

Figure 9. SEM images of the Pt | BCZY27 | LSM/BCZY27 cell after electrolysis and co-electrolysis testing: fracture cross-section view of (a) the porous Pt layer and dense electrolyte interface, (b) the porous LSM/BCZY27 backbone and dense electrolyte, (c) magnification view of the composite backbone infiltrated with Pr_2O_7-CeO_2 nanoparticles and (d) XRD pattern of the Pr_2O_7-CeO_2-infiltrated activation layer.

XRD analysis of the LSM/BCZY27 infiltrated with the catalyst after electrolsysis and co-electrolysis testing (Figure 9d) revealed that the Pr_2O_7-CeO_2 nanoparticles are present in

the anode and that there is no evidence of impurity phases. No secondary phases related to the formation of carbonates or hydroxides are detected.

4. Conclusions

A model electrolyte-supported electrolysis cell was manufactured comprising of a 500 μm-thick $BaCe_{0.2}Zr_{0.7}Y_{0.1}O_{3-\delta}$ electrolyte, a porous Pt anode and a composite cathode made of $La_{0.8}Sr_{0.2}MnO_{3-\delta}$ and BCZY27 (60/40 vol/vol) that was catalytically activated with Pr_2O_7-CeO_2 nanoparticles. The cell was tested in different gas environments, i.e. varying the water concentration in the cathode and CO_2 concentration in the anode.

Despite the high area specific resistance exhibited by the cells due to the electrolyte thickness and non-optimized reference Pt anode, interesting effects in the electrochemistry were found. The electrolysis mode characterization highlighted the positive effect of the H_2O concentration in the anode and the CO_2 presence in the cathode. Higher H_2O and CO_2 concentrations allow for operation at higher current densities giving rise to lower overpotential and, consequently, substantially improving the Faradaic efficiency of the cell.

Water electrolysis was performed at 700 ºC and Faradaic efficiency ranged between 7 and 21% when 3% H_2O was fed into the anode. Significant improvement up to 39% was observed at 10.4 mA/cm^2 by increasing the H_2O concentration to 7.5%. The low Faradaic efficiency is related to the electronic leakage in the electrolyte, partly due to the insufficient oxide hydration and the high built-up overpotential. In order to achieve higher Faradaic efficiencies, the thickness of the electrolyte should be significantly reduced, the cathode optimized and the electrolysis cell operated at high steam concentrations in the anode.

The thickness of the electrolyte can be reduced by the fabrication of cathode-supported cells where the cathode is normally composed of BCZY and NiO (cer-met), these are analogous to anode-supported cells in SOFCs. The reduction of NiO to metallic Ni gives rise to a highly conducting phase [41]. In addition, Ni-cermet cells exhibit strong performance for CO_2/H_2O co-electrolysis [10],[42].

A co-electrolysis test carried out at 700 ºC with 7.5% H_2O demonstrated the positive effect of CO_2 has on the cell resistance. Co-feeding of H_2 and CO_2 to the cathode revealed that the CO_2 hydrogenation rate to CO via RWGS reaction is boosted when current was applied, even at minor current densities. The built-up electrical field in the cathode

modifies the Pt surface and electronic state causing faster kinetics and, probably, the creation of additional H_2 spillover pathways. This effect was previously described in Pt for other surface processes and is coined as the NEMCA effect. In addition, the mixed protonic oxide-ionic conductivity offers the possibility of further control of the CO/H_2 ratio in the produced dry hydrogen in the PCEC cathode.

Acknowledgements

Financial support by the Spanish Government (SEV-2016-0683, Project ENE2014-57651 and IJCI-2016-28330 grants) and by the EU through FP7 Electra Project (Grant Agreement 621244) is gratefully acknowledged. The support of the microscopy service at Universitat Politècnica de València (UPV) for the SEM analysis is recognized.

5. References

[1] A. Brisse, J. Schefold, M. Zahid, High temperature water electrolysis in solid oxide cells, International Journal of Hydrogen Energy 33(20) (2008) 5375-5382.

[2] M. Ni, M.K.H. Leung, D.Y.C. Leung, Technological development of hydrogen production by solid oxide electrolyzer cell (SOEC), International Journal of Hydrogen Energy 33(9) (2008) 2337-2354.

[3] A. Hauch, S.D. Ebbesen, S.H. Jensen, M. Mogensen, Highly efficient high temperature electrolysis, Journal of Materials Chemistry 18(20) (2008) 2331-2340.

[4] C. Duan, J. Tong, M. Shang, S. Nikodemski, M. Sanders, S. Ricote, A. Almansoori, R. O'Hayre, Readily processed protonic ceramic fuel cells with high performance at low temperatures, Science 349(6254) (2015) 1321-1326.

[5] H. Iwahara, High temperature proton conducting oxides and their applications to solid electrolyte fuel cells and steam electrolyzer for hydrogen production, Solid State Ionics 28-30 (1988) 573-578.

[6] N. Bausá, C. Solís, R. Strandbakke, J.M. Serra, Development of composite steam electrodes for electrolyzers based on barium zirconate, Solid State Ionics 306(Supplement C) (2017) 62-68.

[7] R. Strandbakke, V.A. Cherepanov, A.Y. Zuev, D.S. Tsvetkov, C. Argirusis, G. Sourkouni, S. Prünte, T. Norby, Gd- and Pr-based double perovskite cobaltites as oxygen electrodes for proton ceramic fuel cells and electrolyser cells, Solid State Ionics 278 (2015) 120-132.

[8] R. Strandbakke, E. Vøllestad, S.A. Robinson, M.-L. Fontaine, T. Norby, Ba0.5Gd0.8La0.7Co2O6-δ Infiltrated in Porous BaZr0.7Ce0.2Y0.1O3 Backbones as Electrode Material for Proton Ceramic Electrolytes, Journal of The Electrochemical Society 164(4) (2017) F196-F202.

[9] E. Ruiz-Trejo, J.T.S. Irvine, Ceramic proton conducting membranes for the electrochemical production of syngas, Solid State Ionics 216 (2012) 36-40.

[10] E. Ruiz-Trejo, J.T.S. Irvine, Electrolysis of CO2 in a proton conducting membrane, Solid State Ionics 252 (2013) 157-164.

[11] T. Pu, W. Tan, H. Shi, Y. Na, J. Lu, B. Zhu, Steam/CO2 electrolysis in symmetric solid oxide electrolysis cell with barium cerate-carbonate composite electrolyte, Electrochimica Acta 190 (2016) 193-198.

[12] C. Graves, S.D. Ebbesen, M. Mogensen, Co-electrolysis of CO2 and H2O in solid oxide cells: Performance and durability, Solid State Ionics 192(1) (2011) 398-403.

[13] S. Escolastico, M. Ivanova, C. Solis, S. Roitsch, W.A. Meulenberg, J.M. Serra, Improvement of transport properties and hydrogen permeation of chemically-stable proton-conducting oxides based on the system BaZr1-x-yYxMyO3-[small delta], RSC Advances 2(11) (2012) 4932-4943.

[14] Y. Yamazaki, R. Hernandez-Sanchez, S.M. Haile, High Total Proton Conductivity in Large-Grained Yttrium-Doped Barium Zirconate, Chemistry of Materials 21(13) (2009) 2755-2762.

[15] J. LÜ, L. Wang, L. Fan, Y. Li, L. Dai, H. Guo, Chemical stability of doped BaCeO3-BaZrO3 solid solutions in different atmospheres, Journal of Rare Earths 26(4) (2008) 505-510.

[16] J.M. Serra, Electrifying chemistry with protonic cells, Nature Energy 4(3) (2019) 178-179.

[17] C. Duan, R. Kee, H. Zhu, N. Sullivan, L. Zhu, L. Bian, D. Jennings, R. O'Hayre, Highly efficient reversible protonic ceramic electrochemical cells for power generation and fuel production, Nature Energy 4(3) (2019) 230-240.

[18] J. Dailly, M. Marrony, BCY-based proton conducting ceramic cell: 1000 h of long term testing in fuel cell application, Journal of Power Sources 240 (2013) 323-327.

[19] M. Marrony, J. Dailly, Advanced Proton Conducting Ceramic Cell as Energy Storage Device, Journal of The Electrochemical Society 164(9) (2017) F988-F994.

[20] J. Dailly, G. Taillades, M. Ancelin, P. Pers, M. Marrony, High performing BaCe0.8Zr0.1Y0.1O3-δ-Sm0.5Sr0.5CoO3-δ based protonic ceramic fuel cell, Journal of Power Sources 361 (2017) 221-226.

[21] J. Dailly, M. Ancelin, M. Marrony, Long term testing of BCZY-based protonic ceramic fuel cell PCFC: Micro-generation profile and reversible production of hydrogen and electricity, Solid State Ionics 306 (2017) 69-75.

[22] K. Xie, Y. Zhang, G. Meng, J.T.S. Irvine, Electrochemical reduction of CO2 in a proton conducting solid oxide electrolyser, Journal of Materials Chemistry 21(1) (2011) 195-198.

[23] S. Ricote, N. Bonanos, H.J. Wang, R. Haugsrud, Conductivity, transport number measurements and hydration thermodynamics of BaCe0.2Zr0.7Y(0.1-xi)Ni xi O(3-delta), Solid State Ionics 185(1) (2011) 11-17.

[24] H. Iwahara, Technological challenges in the application of proton conducting ceramics, Solid State Ionics 77 (1995) 289-298.

[25] K.H. Ryu, S.M. Haile, Chemical stability and proton conductivity of doped BaCeO3–BaZrO3 solid solutions, Solid State Ionics 125(1) (1999) 355-367.

[26] A.K. Baral, S. Choi, B.K. Kim, J.-H. Lee, Processing and characterizations of a novel proton-conducting BaCe0.35Zr0.50Y0.15O3-δ electrolyte and its nickel-based anode composite for anode-supported IT-SOFC, Materials for Renewable and Sustainable Energy 3(4) (2014) 35.

[27] S.H. Morejudo, R. Zanón, S. Escolástico, I. Yuste-Tirados, H. Malerød-Fjeld, P.K. Vestre, W.G. Coors, A. Martínez, T. Norby, J.M. Serra, C. Kjølseth, Direct conversion of methane to aromatics in a catalytic co-ionic membrane reactor, Science 353(6299) (2016) 563-566.

[28] H. Malerød-Fjeld, D. Clark, I. Yuste-Tirados, R. Zanón, D. Catalán-Martinez, D. Beeaff, S.H. Morejudo, P.K. Vestre, T. Norby, R. Haugsrud, J.M. Serra, C. Kjølseth, Thermo-electrochemical production of compressed hydrogen from methane with near-zero energy loss, Nature Energy 2(12) (2017) 923-931.

[29] P. Babilo, S.M. Haile, Enhanced Sintering of Yttrium-Doped Barium Zirconate by Addition of ZnO, Journal of the American Ceramic Society 88(9) (2005) 2362-2368.

[30] E. Rebollo, C. Mortalo, S. Escolastico, S. Boldrini, S. Barison, J.M. Serra, M. Fabrizio, Exceptional hydrogen permeation of all-ceramic composite robust membranes based on BaCe0.65Zr0.20Y0.15O3-[small delta] and Y- or Gd-doped ceria, Energy & Environmental Science 8(12) (2015) 3675-3686.

[31] N. Bausá, J.M. Serra, RSC Advances (2019).

[32] S. Ricote, N. Bonanos, M.C. Marco de Lucas, G. Caboche, Structural and conductivity study of the proton conductor BaCe(0.9−x)ZrxY0.1O(3−δ) at intermediate temperatures, Journal of Power Sources 193(1) (2009) 189-193.

[33] T. Kobayashi, K. Kuroda, S. Jeong, H. Kwon, C. Zhu, H. Habazaki, Y. Aoki, Analysis of the Anode Reaction of Solid Oxide Electrolyzer Cells with BaZr0.4Ce0.4Y0.2O3-δ Electrolytes and Sm0.5Sr0.5CoO3-δ Anodes, Journal of The Electrochemical Society 165(5) (2018) F342-F349.

[34] S. Akoshima, M. Oishi, K. Yashiro, K. Sato, J. Mizusaki, Reaction kinetics on platinum electrode / yttrium-doped barium cerate interface under H2–H2O atmosphere, Solid State Ionics 181(3) (2010) 240-248.

[35] L. Navarrete, PhD Thesis: New electrochemical cells for energy conversion and storage, Instituto de Tecnología Química, Instituto de Tecnología Química (UPV-CSIC), 2017.

[36] M. Ouzounidou, A. Skodra, C. Kokkofitis, M. Stoukides, Catalytic and electrocatalytic synthesis of NH3 in a H+ conducting cell by using an industrial Fe catalyst, Solid State Ionics 178(1) (2007) 153-159.

[37] N.A. Anastasijevic, NEMCA—From discovery to technology, Catalysis Today 146(3) (2009) 308-311.

[38] I. Kalaitzidou, A. Katsaounis, T. Norby, C.G. Vayenas, Electrochemical promotion of the hydrogenation of CO2 on Ru deposited on a BZY proton conductor, Journal of Catalysis 331 (2015) 98-109.

[39] L. Navarrete, C. Solis, J.M. Serra, Boosting the oxygen reduction reaction mechanisms in IT-SOFC cathodes by catalytic functionalization, Journal of Materials Chemistry A 3(32) (2015) 16440-16444.

[40] J. Garcia-Fayos, R. Ruhl, L. Navarrete, H.J.M. Bouwmeester, J.M. Serra, Enhancing oxygen permeation through Fe2NiO4-Ce0.8Tb0.2O2-[small delta] composite membranes using porous layers activated with Pr6O11 nanoparticles, Journal of Materials Chemistry A 6(3) (2018) 1201-1209.

[41] W.G. Coors, A. Manerbino, Characterization of composite cermet with 68wt.% NiO and BaCe0.2Zr0.6Y0.2O3−δ, Journal of Membrane Science 376(1) (2011) 50-55.

[42] G. Wu, K. Xie, Y. Wu, W. Yao, J. Zhou, Electrochemical conversion of H2O/CO2 to fuel in a proton-conducting solid oxide electrolyser, Journal of Power Sources 232 (2013) 187-192.

SUPPORTING INFORMATION

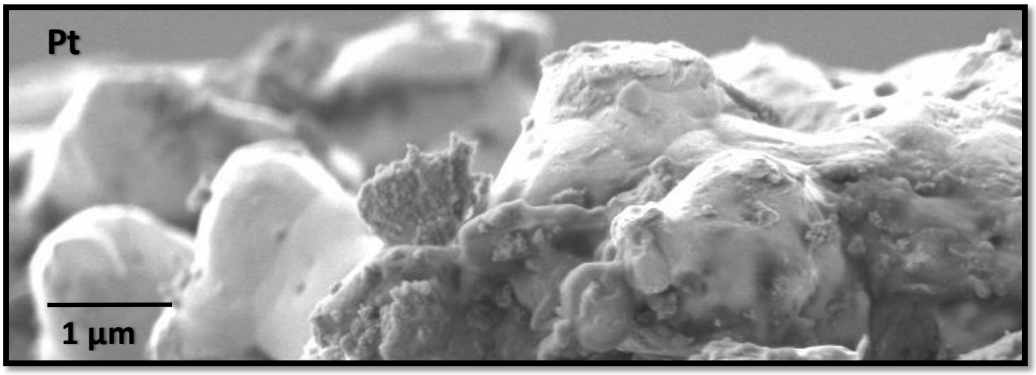

Supporting Figure S1. SEM image of Pt layer after sintering at 1100 ºC for 2 hours.

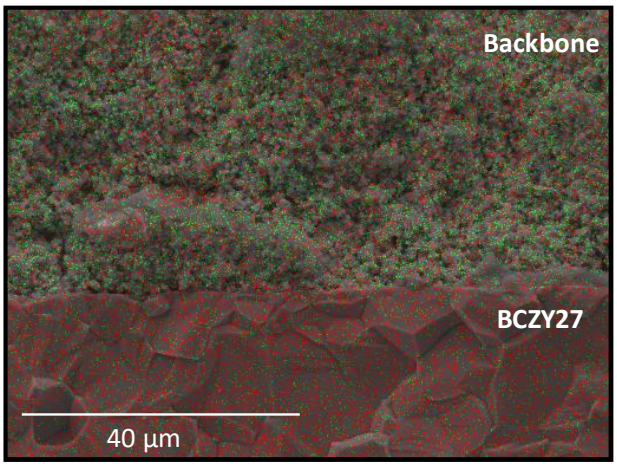

Supporting Figure S2. SEM-EDX mapping of the Pr (green) and Ce (red) elements.

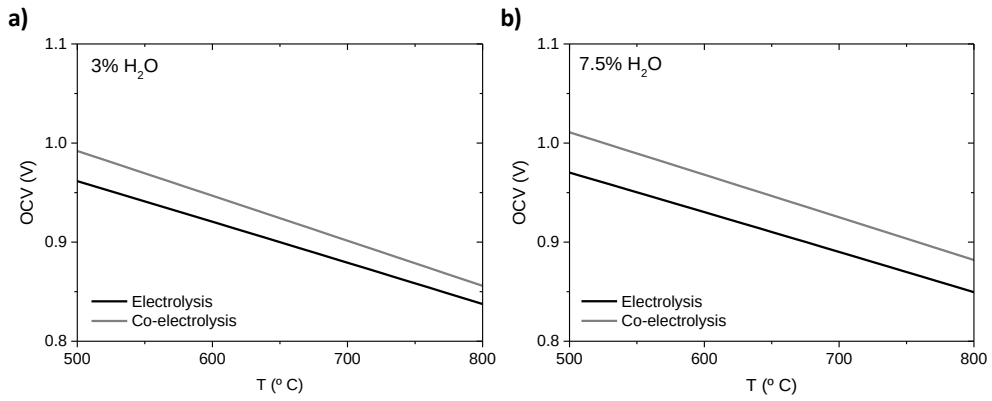

Supporting Figure S3. Expected OCV values in electrolysis and co-electrolysis mode at atmospheric pressure and different temperature and steam concentrations: 3% H_2O (a) and 7.5% H_2O (b)